

Systematic Modulation of Quantum (Electron) Tunneling Behavior by Atomic Layer Deposition on Nanoparticulate SnO₂ and TiO₂ Photoanodes

Chaiya Prasittichai,^{†,§,||} Jason R. Avila,^{†,||} Omar K. Farha,^{*,†} and Joseph T. Hupp^{*,†,‡}

[†]Department of Chemistry and Argonne-Northwestern Solar Energy Research (ANSER) Center, Northwestern University, Evanston, Illinois 60208, United States

[‡]Argonne National Laboratory, Argonne, Illinois 60439, United States

S Supporting Information

ABSTRACT: Ultrathin films of TiO₂, ZrO₂, and Al₂O₃ were conformally created on SnO₂ and TiO₂ photoelectrodes via atomic layer deposition (ALD) to examine their influence upon electron transfer (ET) from the electrodes to a representative molecular receptor, I₃⁻. Films thicker than 2 Å engender an exponential decrease in ET time with increasing film thickness, consistent with tunneling theory. Increasing the height of the barrier, as measured by the energy difference between the transferring electron and the bottom of the conduction band of the barrier material, results in steeper exponential drops in tunneling rate or probability. The variations are quantitatively consistent with a simple model of quantum tunneling of electrons through square barriers (i.e., barriers of individually uniform energy height) that are characterized by individually uniform physical thickness. The findings demonstrate that ALD is a remarkably uniform and precise method for modifying electrode surfaces and imply that standard tunneling theory can be used as a quantitative guide to intentionally and predictively modulating rates of ET between molecules and electrodes.

Electron transfer (ET) via quantum tunneling has been extensively studied for a variety of organic, biological, and metal-ion-containing chemical systems.^{1–5} Often these studies focus on the separation of a photoexcited donor species from an electron acceptor (or vice versa) by a well-defined matrix, e.g., frozen solvent, rigid organic linker, or spatially fixed biological medium.^{6–8} In other studies, electrons are transferred from an electrode, through a predefined organic tether, to a pendant molecule (or vice versa). As Gray et al. have noted, systematic control over electron tunneling has enabled molecular reactivity (mainly in biological and organic environments) to be tuned over a dynamic range of 11 orders of magnitude or more.^{2,9} Thus, electron tunneling is among the kinetically most versatile tools available to scientists or nature herself for modulating chemical reactivity.

Despite broad investigation with carbon-based media, electron tunneling through strictly inorganic media to solvated, redox-active, molecular species, has been comparatively ill explored—at least in well-defined and quantitative fashion. In principle, coating an electrode, such as the nanoparticulate and

semiconducting photoanode of a dye-sensitized solar cell (DSC), with a layer of a second metal-oxide, such as ZrO₂ or Al₂O₃, would be an attractive approach to remedying this deficiency. Thus, one could systematically modulate ET to molecular species by creating tunneling barriers of well-defined thickness and composition. While a variety of coating methods have been considered, the technique referred to as “dip-coating” has been commonly utilized to apply barrier layers on electrodes.^{10–12} However, this method typically creates layers with irregular, unpredictable thicknesses, as well as pinholes that can provide undesired, additional conduits for ET.¹³

In contrast, atomic layer deposition (ALD),^{14–19} which typically entails the exposure of a surface alternately to a vapor-phase metal precursor and an oxygen source, is able to generate pinhole-free metal-oxide films with angstrom-scale thickness control due to its self-terminating growth mechanism. In addition, the gas-phase nature of the delivery of film building blocks enables conformal coating of even high-surface area materials. These features make ALD an ideal method for applying ultrathin barrier layers to high surface area platforms.^{20–22} This method has been utilized by our lab (and others^{22–24}) with DSCs to retard deleterious interception of photoinjected electrons within sensitized semiconductor electrodes by molecular redox shuttles.^{25–29} Interestingly, for the case of ALD-grown Al₂O₃ on SnO₂ photoelectrodes, a single cycle (~30–40% of a monolayer, fixed by the footprint of the ALD precursor (CH₃)₃Al)^{14,15} decreases the rate of back-ET from the electrode to a molecular acceptor by ~100 fold;²⁶ thicker ALD-applied films further decrease the rate, but in a less spectacular fashion that appears consistent with distance-modulated electron tunneling.

As suggested by Figure 1, the rate or probability of electron tunneling from an electrode, through a barrier, and into a molecular acceptor is anticipated to depend on both the barrier thickness (tunneling distance, *d*) and the barrier height, ΔE , relative to the energy of the tunneling electron. For a simple square barrier, the ET rate (or rate constant, k_{ET}) will decrease exponentially with increasing tunneling distance/layer thickness:

$$k_{ET} = k_{ET}^0 e^{-\beta d} \quad (1)$$

Received: August 29, 2013

Published: October 22, 2013

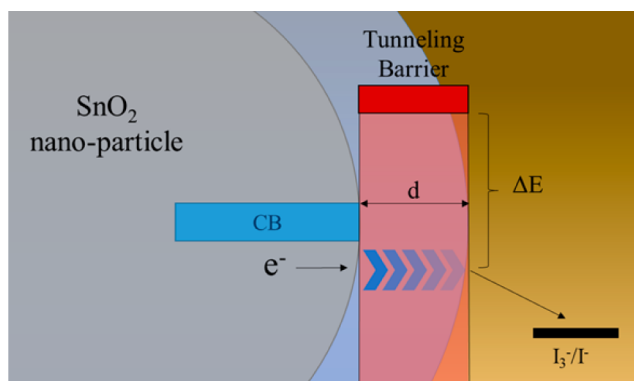


Figure 1. Proposed schematic of electron tunneling through an insulating barrier layer on a nanoparticulate tin-oxide photoelectrode in contact with a solution containing triiodide as an electron acceptor.

The tunneling parameter, β , describes the steepness of the exponential decrease; large β values are characteristic of strong distance dependence, while small values indicate weak dependence. In the case of a square barrier, the magnitude of β is anticipated to scale as $(\Delta E)^{1/2}$.² Thus, barrier layers that feature high conduction-band-edge energies (E_{cb}) should yield large β values, while those with lower band-edge energies should yield smaller β values, i.e., shallower fall-offs in tunneling rate with barrier-defined electrode/molecule separation distance.

The broad chemical compositional viability of ALD suggests that its application to conformal growth of barrier layers on photoelectrodes could enable tunneling to molecular acceptors, through purely inorganic media, to be systematically explored. Herein we describe such studies. Specifically, we examine tunneling in the context of DSCs that feature high-area SnO_2 electrodes. Semiconducting tin-oxide is an ideal source for tunneling electrons because its conduction-band-edge energy lies significantly below those of most other ALD accessible, wide-bandgap metal-oxides; thus, tunable barriers can be readily introduced. For the materials examined here the ordering of band-edge energies is: $\text{SnO}_2 < \text{TiO}_2 < \text{ZrO}_2 \ll \text{Al}_2\text{O}_3$. For similar reasons, we also examined TiO_2 -based photoelectrodes featuring ultrathin conformal coatings of either ZrO_2 or Al_2O_3 as tunneling barriers.

Rates of ET from photoelectrodes, through metal-oxide barrier layers, to a representative solution-phase molecular acceptor, triiodide, were determined by measuring survival times, τ_n , of photoinjected electrons within electrodes. These times are readily obtained by tracking decays in DSC open-circuit voltage (V_{OC}) after interrupting illumination. The survival time (decay time) is inversely related to the ET rate and, therefore, k_{ET} . The open-circuit voltage, at any specified instant, defines the energy of the transferring electron relative to the potential of the DSC counter-electrode (i.e., the Nernst potential of the molecular acceptor and its reduced counterpart, in this case iodide).^{30,31} The time-evolving value of ΔE (Figure 1) is simply the difference between the known value of E_{cb} for the barrier-layer material of interest and the measured value (also time-evolving) of V_{OC} .³²

Figure 2 shows survival times as a function of V_{OC} for dye-injected electrons within a naked SnO_2 electrode and within analogous photoelectrodes coated with a single cycle (a fraction of a monolayer) of TiO_2 , ZrO_2 , or Al_2O_3 . These modest modifications engender substantial changes in survival times (τ_n values) for injected electrons. The relative magnitudes of the

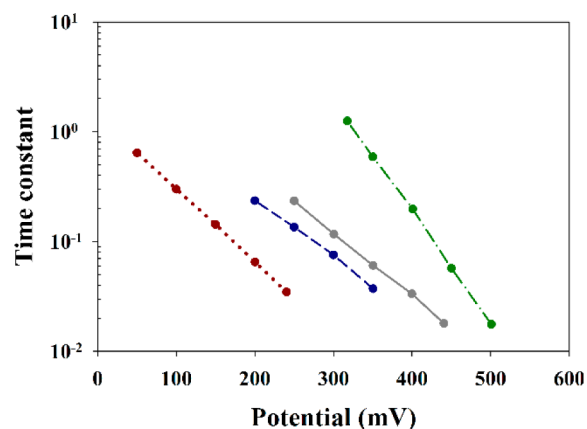


Figure 2. Photovoltage decays for cells containing naked SnO_2 (dotted red line), SnO_2 coated with 1 cycle of TiO_2 (dashed blue line), 1 cycle of ZrO_2 (solid gray line), or 1 cycle of Al_2O_3 (dot-dash-dot green line). Initial light intensity = 1 sun.

changes are somewhat dependent on the V_{OC} value at which systems are compared. Clearly, however, survival times increase (and k_{ET} values decrease) in the order: no ALD \rightarrow TiO_2 ALD \rightarrow ZrO_2 ALD \rightarrow Al_2O_3 ALD. It has been suggested that metal-oxide coating induced increases in electron survival times are due to shifts of the conduction-band-edge energy of the underlying electrode material to higher absolute energy (more negative electrochemical potential).^{33,34} We have shown elsewhere, however, that for tunneling purposes these shifts are negligible (i.e., a few tens of mV or less for alumina on SnO_2 and alumina on TiO_2).^{26,35}

Figure 3 illustrates how the rate of ET ($\propto 1/\tau_n$) from tin-oxide to solution-phase triiodide varies with the average

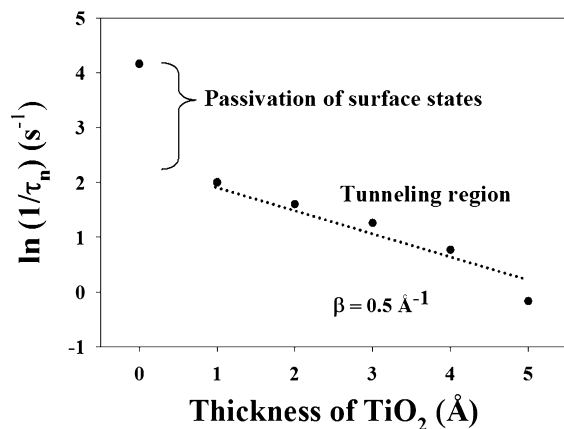


Figure 3. Plot of the natural log of the inverse of the electron interception time ($1/\tau_n$) for injected electrons in SnO_2 electrodes coated with TiO_2 blocking layer. The slope of the line (excluding zero thickness; see text) indicates the β value. To minimize data extrapolation, interception times (survival times) at $V_{OC} = 300$ mV were chosen for SnO_2 base electrodes. For TiO_2 electrodes (zirconia or alumina coatings; see SI) measured or extrapolated times at $V_{OC} = 600$ mV were used.

thickness of a TiO_2 coating. As previously found for Al_2O_3 functionalization of SnO_2 , the first ALD cycle of TiO_2 exerts a greater effect upon $\ln(1/\tau_n)$ than do subsequent cycles.²⁶ One interpretation is that TiO_2 installed in the first cycle serves to passivate sub-band-edge surface states that otherwise facilitate

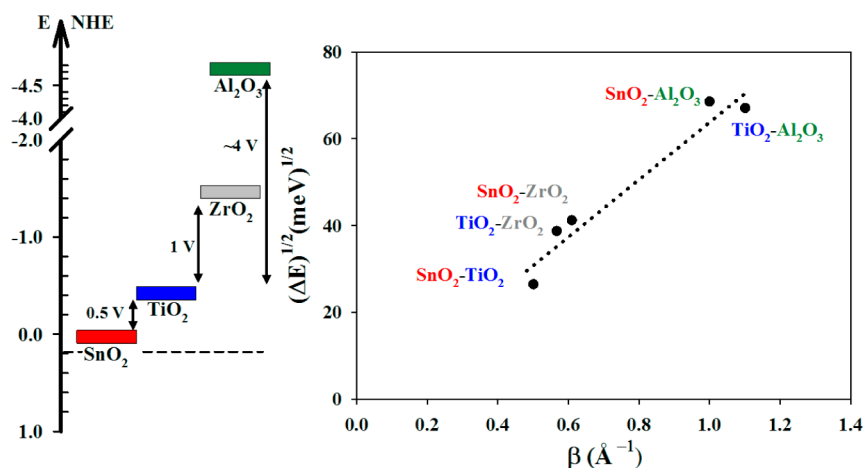


Figure 4. (Left) Energy diagram of metal-oxide conduction-band-edge positions. The dashed line represents the potential of the transferring electron. (Right) Plot of the square root of the tunneling barrier height vs the experimentally determined value of the tunneling attenuation parameter β for various source-electrode/barrier-layer combinations. The slope of the plot is $65 \pm 9 \text{ (meV)}^{1/2} \text{ \AA}$.

(catalyze) electron interception. The nature of these states is still uncertain, but we speculate that they arise from “incorrect” coordination of Sn(IV) on the surface of the electrode.^{25,26,35} (For example, one or more aquo or hydroxo ligands could supplant oxo ions in the tin coordination sphere.³⁶)

Regardless of the explanation for the effects of the first ALD cycle, the log-normal data presentation in Figure 3 illustrates that subsequent cycles engender an exponential falloff in ET rate with increasing barrier-layer thickness. This behavior is consistent with control of ET kinetics by electron tunneling. Recalling that k_{ET} and τ_n are inversely related, a fit of the data to eq 1 yields a tunneling parameter, β , of 0.5. Plots of $\ln(1/\tau_n)$ vs barrier thickness, and resulting values of β , for other photoelectrode/ALD-coating combinations can be found in the Supporting Information (SI; Figure S2).

With these results in hand, the dependence of β on the height of the putative tunneling barrier can be determined. Figure 4 shows that β correlates reasonably well with $(\Delta E)^{1/2}$, as expected if tunneling controls ET in these systems.³⁷ The observed slope of $65 \pm 9 \text{ (meV)}^{1/2} \text{ \AA}$ is in excellent agreement with slope expected from standard tunneling theory, i.e. $62 \text{ (meV)}^{1/2} \text{ \AA}$. Similarly, the observed small intercept is in good agreement with the intercept of zero expected from tunneling theory. Taken together, these results clearly establish that ET from photoelectrodes and through inorganic barrier layers to molecular acceptors is governed by electron tunneling.

To ascertain whether ALD layers function as blocking layers even under dark conditions, we additionally examined a representative series of ALD-coated tin-oxide electrodes (specifically, alumina coated) by electrochemical impedance spectroscopy (EIS).^{38,39} As used here, EIS is a dark measurement, with electrons injected by a potentiostat rather than by photoexcited dye molecules. As shown in Figure 5, each of four cells yields a large arc at low frequencies (10^{-2} – 10^3 Hz). The arc is attributable to charge transfer to triiodide. As each cycle of Al_2O_3 is added, the charge-transfer resistance, which scales roughly as the diameter of the large semicircle and which is inversely proportional to the ET rate, increases significantly. The observed behavior corroborates the photocell derived picture of ALD ad-layers as electron-tunneling barriers.¹⁴

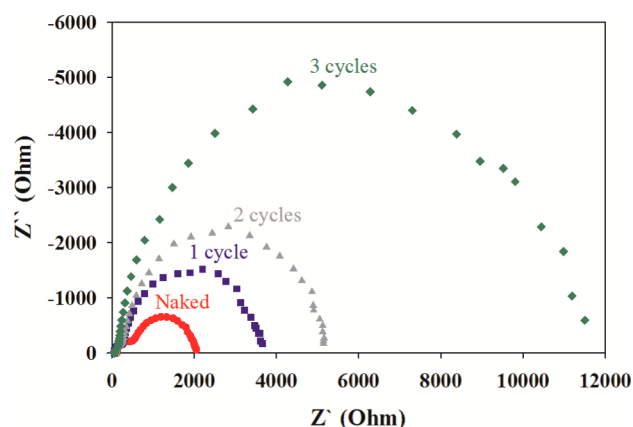


Figure 5. Nyquist plots for dark cells containing naked SnO_2 (red circles) and SnO_2 coated with 1 (blue squares), 2 (gray triangles), and 3 (green diamonds) cycles of Al_2O_3 ; dc potential = 300 mV.

In conclusion, we demonstrate that tunneling controlled ET through strictly inorganic media to solution-phase molecular acceptors can be quantitatively examined by enlisting DSC photoelectrodes as electron sources and conformally coating them with candidate barrier layers via ALD. The candidate materials examined—various wide-bandgap metal-oxides—behave in near textbook fashion as media for electron tunneling. ET rates proved to be broadly tunable based on both modulation of tunneling distance (barrier layer thickness) and on manipulation of barrier energy height. Since tunneling probabilities change sharply with tunneling distance, the observed quantitative agreement with theory implies that ALD is delivering exceptionally uniform and pinhole-free coatings, despite the fact that the underlying electrodes are porous, nanoparticulate, and comparatively thick overall ($\sim 4000 \text{ nm}$). The findings additionally imply that standard tunneling theory can be used as a quantitative guide to intentionally and predictively modulating rates of ET between molecules and electrodes. This capability could be of substantial value in optimizing the efficiencies of DSCs,^{22–29} hybrid dye cells,²⁷ heterogeneous redox and photoredox catalysts,^{40–42} and related systems. Our own ongoing studies are focused on gaining a similarly detailed understanding of electron tunneling through hybrid organic/inorganic barrier layers.⁴³

■ ASSOCIATED CONTENT

S Supporting Information

Experimental conditions, cells lifetimes, and tunneling constants. This material is available free of charge via the Internet at <http://pubs.acs.org>.

■ AUTHOR INFORMATION

Corresponding Authors

o-farha@northwestern.edu

j-hupp@northwestern.edu

Present Address

[§]Department of Chemical Engineering, Stanford University, Stanford, California 94305, United States.

Author Contributions

^{||}These authors contributed equally.

Notes

The authors declare no competing financial interest.

■ ACKNOWLEDGMENTS

We thank Dr. Jeffery Elam at Argonne National Laboratory for allowing us to deposit TiO₂ with TiCl₄. C.P. acknowledges funding from the Strategic Fellowships for Frontier Research Networks from the Commission on Higher Education, Thailand for his graduate fellowship. J.R.A. acknowledges Shelley Zaleski for her consultation with theoretical calculations. J.T.H. gratefully acknowledges the ANSER Center, an Energy Frontier Research Center funded by the U.S. Department of Energy, Office of Science, Office of Basic Energy Sciences, under award no. DE-SC0001059 for funding.

■ REFERENCES

- (1) Davis, W. B.; Svec, W. A.; Ratner, M. A.; Wasielewski, M. R. *Nature* **1998**, *396*, 60–63.
- (2) Edwards, P. P.; Gray, H. B.; Lodge, M. T. J.; Williams, R. J. P. *Angew. Chem., Int. Ed.* **2008**, *47*, 6758–6765 and references therein.
- (3) Vargo, M. L.; Gulka, C. P.; Gerig, J. K.; Manieri, C. M.; Dattelbaum, J. D.; Marks, C. B.; Lawrence, N. T.; Trawick, M. L.; Leopold, M. C. *Langmuir* **2010**, *26*, 560–569.
- (4) Bell, R. P. *The Tunneling Effect in Chemistry*; Chapman and Hall: New York, 1980.
- (5) Hankache, J.; Wenger, O. *Chem. Rev.* **2011**, *111*, 5138–5178.
- (6) Sikes, H. D.; Smalley, J. F.; Dudek, S. P.; Cook, A. R.; Newton, M. D.; Chidsey, C. E. D.; Feldberg, S. W. *Science* **2001**, *291*, 1519–1523.
- (7) Cheng, J.; Robinson, D. B.; Cicero, R. L. *J. Phys. Chem. B* **2001**, *105*, 10900–10904.
- (8) Zhao, J. W.; Uosaki, K. *J. Phys. Chem. B* **2004**, *108*, 17129–17135.
- (9) Gray, H. B.; Winkler, J. R. *Q. Rev. Biophys.* **2003**, *36*, 341–372.
- (10) Zaban, A.; Chen, S. G.; Chappel, S.; Gregg, B. A. *Chem. Commun.* **2000**, 2231–2232.
- (11) Palomares, E.; Clifford, J. N.; Haque, S. A.; Lutz, T.; Durrant, J. *J. Chem. Chem. Soc.* **2003**, *125*, 475–482.
- (12) Tiwana, P.; Docampo, P.; Johnston, M. B.; Herz, L. M.; Snaith, H. J. *Energy Environ. Sci.* **2012**, *5*, 9566–9573.
- (13) Guo, J.; She, C.; Lian, T. *J. Phys. Chem. C* **2007**, *111*, 8979–8987.
- (14) George, S. M. *Chem. Rev.* **2010**, *110*, 111–131.
- (15) Miikulainen, V.; Leskela, M.; Ritala, M.; Puurunen, R. L. *J. Appl. Phys.* **2013**, *113*, 021301–21402.
- (16) Chen, P.; Mitsui, T.; Farmer, D. B.; Golovchenko, J.; Gordon, R. G.; Branton, D. *Nano Lett.* **2004**, *4*, 1333–1337.
- (17) Bakke, J. R.; Pickrahn, K. L.; Brennan, T. P.; Bent, S. F. *Nanoscale* **2011**, *3*, 3482–3508.
- (18) Elam, J. W.; Dasgupta, N. P.; Prinz, F. B. *MRS Bull.* **2011**, *36*, 899–906.
- (19) Elam, J. W.; Routkevitch, D.; Mardilovich, P. P.; George, S. M. *Chem. Mater.* **2003**, 3507–3517.
- (20) Gubbala, S.; Chakrapani, V.; Kumar, V.; Sunkara, M. K. *Adv. Func. Mater.* **2008**, *18*, 2411–2418.
- (21) Lin, C.; Tsai, F.-Y.; Lee, M.-H.; Lee, C.-H.; Tien, T.-C.; Wang, L.-P.; Tsai, S.-Y. *J. Mater. Chem.* **2009**, *19*, 2999–3003.
- (22) Klahr, B. M.; Hamann, T. W. *J. Phys. Chem. C* **2009**, *113*, 14040–14045.
- (23) Chandiran, A. K.; Tetreault, N.; Humphry-Baker, R.; Kessler, F.; Baranoff, E.; Yi, C.; Nazeeruddin, M. K.; Gratzel, M. *Nano Lett.* **2012**, *12*, 3941–3947.
- (24) Law, M.; Greece, L. E.; Radenovic, A.; Kuykendall, T.; Liphardt, J.; Yang, P. *J. Phys. Chem. B* **2006**, *110*, 22652–22663.
- (25) DeVries, M. J.; Pellin, M. J.; Hupp, J. T. *Langmuir* **2010**, *26*, 9082–9087.
- (26) Prasittichai, C.; Hupp, J. T. *J. Phys. Chem. Lett.* **2010**, *1*, 1611–1615.
- (27) Li, T.; Góes, M.; Santiago, F. F.; Bisquert, J.; Bueno, P. R.; Prasittichai, C.; Hupp, J. T.; Marks, T. J. *J. Phys. Chem. C* **2009**, *113*, 18385–18390.
- (28) Williams, V. O.; Jeong, N. C.; Prasittichai, C.; Farha, O. K.; Pellin, M. J.; Hupp, J. T. *ACS Nano* **2012**, *12*, 6185–6196.
- (29) Li, T. C.; Fabregat-Santiago, F.; Farha, O. K.; Spokoyny, A. M.; Raga, S. R.; Bisquert, J.; Mirkin, C. A.; Marks, T. J.; Hupp, J. T. *J. Phys. Chem. C* **2011**, *115*, 11257–11264.
- (30) Bisquert, J.; Zaban, A.; Greenshtein, M.; Mora-Seró, J. *Am. Chem. Soc.* **2004**, *126*, 13550–13559.
- (31) For the redox electrolyte concentrations and the solvent composition used here, the Nernst potential is +700 mV vs a Ag/AgCl reference electrode and +500 mV vs E_{cb} (SnO₂). See: Boschloo, G.; Hagfeldt, A. *Acc. Chem. Res.* **2009**, *42*, 1819–1826.
- (32) Measurements here were made under conditions where back ET to the sensitizing dye is negligible. If ET proceeds first by thermal population of the photoelectrode's conduction band, then a more appropriate choice for ΔE would be the difference in E_{cb} values for the barrier layer material and the photoelectrode material. As shown in the SI, this refinement has little effect upon subsequent conclusions regarding degree of experimental agreement with tunneling theory.
- (33) Antila, L. J.; Heikkilä, M. J.; Humalain, N.; Laitinen, M.; Linko, V.; Jalkanen, P.; Toppari, J.; Aumanen, V.; Kemell, M.; Myllyperki, P.; Honkala, K.; Leskela, M.; Korppi-Tommola, J. E. I. *J. Phys. Chem. C* **2011**, 16720–16729.
- (34) Antila, L. J.; Heikkilä, M. J.; Aumanen, V.; Kemell, M.; Myllyperki, P.; Leskela, M.; Korppi-Tommola, J. E. I. *J. Phys. Chem. Lett.* **2010**, *1*, 536–539.
- (35) Katz, M.; Vermeer, M.; Farha, O.; Pellin, M.; Hupp, J. *Langmuir* **2012**, *29*, 806–814.
- (36) If the speculation is correct, surface aquo and hydroxo groups should preferentially react with ALD precursors, presumably resulting in restoration of an all-oxo Sn(IV) coordination environment.
- (37) Consistent with the correlation, if we plot $\log \beta$ vs $\log \Delta E$ we obtain we obtain a best-fit slope of 0.43 ± 0.07 . This constitutes an independent and empirical (i.e., model-free) evaluation of the exponent for ΔE .
- (38) Biquert, J.; Vikherenk, V. S. *J. Phys. Chem. B* **2004**, *108*, 2313–2322.
- (39) Biquert, J. *J. Electroanal. Chem.* **2010**, *646*, 43–51.
- (40) Liu, F.; Cardolaccia, T.; Hornstein, B. J.; Schoonover, J. R.; Meyer, T. J. *J. Am. Chem. Soc.* **2007**, *129*, 2446–2447.
- (41) Youngblood, W. J.; Lee, S. A.; Kobayashi, Y.; Hernandez-Pagan, E. A.; Hoertz, P. G.; Moore, T. A.; Moore, A. L.; Gust, D.; Mallouk, T. E. *J. Am. Chem. Soc.* **2009**, *131*, 926–927.
- (42) Huang, Z.; Luo, Z.; Geletii, J. W. V.; Yin, Q.; Wu, D.; Hou, Y.; Ding, Y.; Song, J.; Musaev, D. G.; Hill, C. L.; Lian, T. *J. Am. Chem. Soc.* **2011**, *133*, 2068–2071.
- (43) Son, H. J.; Wang, X.; Prasittichai, C.; Jeong, N. C.; Aaltonen, T.; Gordon, R. G.; Hupp, J. T. *J. Am. Chem. Soc.* **2012**, *134*, 9537–9540.